UNIVERSITY OF LEEDS

This is a repository copy of *Optimized Reforming of Biomass Derived Gas Based on Thermodynamic and Kinetics Analysis with Activated Carbon Fibers Supported Ni-Al_2O_3*.

White Rose Research Online URL for this paper:
https://eprints.whiterose.ac.uk/156820/

Version: Accepted Version

Article:
Yu, L, Song, M, Williams, PT orcid.org/0000-0003-0401-9326 et al. (1 more author) (2020) Optimized Reforming of Biomass Derived Gas Based on Thermodynamic and Kinetics Analysis with Activated Carbon Fibers Supported Ni-Al_2O_3. BioEnergy Research, 13. pp. 581-590. ISSN 1939-1234

https://doi.org/10.1007/s12155-019-10087-6

© Springer Science+Business Media, LLC, part of Springer Nature 2020. This is an author produced version of a paper published in Bioenergy Research. Uploaded in accordance with the publisher's self-archiving policy.

Reuse
Items deposited in White Rose Research Online are protected by copyright, with all rights reserved unless indicated otherwise. They may be downloaded and/or printed for private study, or other acts as permitted by national copyright laws. The publisher or other rights holders may allow further reproduction and re-use of the full text version. This is indicated by the licence information on the White Rose Research Online record for the item.

Takedown
If you consider content in White Rose Research Online to be in breach of UK law, please notify us by emailing eprints@whiterose.ac.uk including the URL of the record and the reason for the withdrawal request.

White Rose university consortium
Universities of Leeds, Sheffield & York

eprints@whiterose.ac.uk
https://eprints.whiterose.ac.uk/

Optimized reforming of biomass derived gas based on thermodynamic and kinetics analysis with activated carbon fibers supported Ni-Al_2O_3

Lei Yu [1], Min Song [1,*], Paul T. Williams [2], Yuexing Wei [1]

1 Ministry of Education of Key Laboratory of Energy Thermal Conversion and Control, School of Energy and Environment, Southeast University, Nanjing, 210096, China

2 School of Chemical & Process Engineering, University of Leeds, Leeds, LS2 9JT, UK

*Correspondence author: minsong@seu.edu.cn;

Abstract

Thermodynamics and kinetics are the two key factors in optimizing the biomass derived gas reforming to obtain syngas. In this study, the effects of components of simulated biomass derived gas (CH_4, CO_2, H_2, CO, N_2 and steam), reforming conditions and different reactions on products distribution were investigated under thermodynamic equilibrium using Gibbs free energy minimization method so as to optimize the reforming conditions and provide theoretical basis for further reforming of biomass derived gas. The results showed that temperature and steam play an important role in manipulating the ratio of H_2/CO during reforming. Changing the temperature and the amount of steam can promote the reverse water-gas shift reaction in different directions thereby the syngas yield can be increased and the H_2/CO ratio can be adjusted so as to meet different application requirements. Furthermore, the macroscopic kinetics analysis with a simple power-law type kinetic equation over our previous reported catalyst Ni-Al_2O_3/ACF (Activated Carbon Fibers) used for the reforming of simulated biomass derived gas was obtained. The influence of carbon fibers on the catalytic performance of nickel-based alumina catalyst was explained in terms of activation energy.

Keywords: Thermodynamic analysis; Biomass; Gasification; Optimum reforming; Kinetics

1 Introduction

Nowadays methane reforming [1, 2], coal gasification [3, 4] and other fossil fuel conversion methods [5] are commonly used for the syngas (CO and H_2) production. However, the limitation of fossil fuel through consideration of sustainability and climate change issues will be a bottleneck for these technologies in the future.

The biomass gasification [6, 7] for syngas production has attracted wide attention because of the renewable and cheap raw materials. Dong et al. [8] and Waheed et al. [9] conducted the gasification of different biomass such as wood sawdust and rice husks for hydrogen production with various nickel based catalysts [10]. Wu et al and Waheed et al [11, 12] showed that steam gasification could reduce the coke on the catalyst surface during gasification compared with the use of CO_2 and air as gasifying agents. However, the gasified gas should be improved to adjust the ratio of H_2/CO [13] by further catalytic reforming. The interaction of various components, different reactions and the influence of reforming parameters in the further reforming process of biomass derived gas were still not revealed thoroughly. To this end, the effects of components, reforming conditions and different reactions on products distribution under thermodynamic equilibrium by Gibbs free energy minimization method will be investigated so as to optimize the reforming conditions and provide theoretical basis for further reforming of biomass derived gas.

In addition, developing a catalyst with great thermal stability and resistance of coke on the surface of catalyst is still a challenging topic [14]. Activated carbon materials used as catalysts or supports for biomass gasification have been reported due to their excellent surface properties [15]. Wang et al. [16] loaded nickel on lignite char via ion-exchange for low-temperature gasification of corn cob to study the effects of different operating conditions on gas yields and carbon distributions. They reported that nickel particles dispersed quite well in the catalyst. To enhance hydrogen production from biomass gasification, Yao et al. [17] used three bio-chars as support to prepare nickel based catalysts for the steam gasification of wheat straw. In our other research, different types of carbon materials such as activated carbon [18] and activated carbon fibers [19, 20] have also been prepared. Among numerous carbon materials, alkaline activated carbon fibers (ACF) have shown particular advantages, including high specific surface area, rich functional groups and abundant basic sites on the surface [21]. In our previous reported research [22], nickel and alumina were co-precipitated together on the surface of ACF to prepare a catalyst (Ni-Al_2O_3/ACF) used for the reforming of simulated biomass derived gas. The catalyst showed excellent catalytic performance especially

for the conversion of CO_2. For these research, the explanation for the catalytic performance of carbon based catalysts is mainly in terms of textural and surface properties. In this work, the properties of carbon based catalyst will be illustrated from the perspective of activation energy with the previous prepared catalyst Ni-Al_2O_3/ACF.

Generally, this work aims to conduct a macroscopic reaction kinetics investigation into the reforming system of simulated biomass derived gas over the catalyst Ni-Al_2O_3/ACF used for gasified biomass product gas reforming. A simple power-law type kinetic equation of the catalyst Ni-Al_2O_3/ACF was calculated and the activation energy of CH_4 and CO_2 in different temperature ranges was illustrated. The novelty of this work also includes the thermodynamic analysis of simulated biomass derived gas reforming to illustrate the effects of different input gas compositions (CH_4, CO_2, H_2, CO and steam) and reforming conditions so as to optimize the reforming of biomass derived gas.

2 Experiment and methodology

2.1 Catalysts preparation

The catalyst Ni-Al_2O_3/ACF was prepared by co-precipitation method. Polyacrylonitrile (PAN) based activated carbon fibers (ACF), nickel nitrate, aluminum nitrate and sodium carbonate were used as the precipitation precursors. The mixed solution of nickel nitrate and aluminum nitrate was co-precipitated with the solution of sodium carbonate by two peristaltic pumps in a beaker placed in magnetic stirrer at 40 ^oC. The ACF was added into the beaker ahead and the intermediate product was co-precipitated on the surface of ACF. After co-precipitation, the precipitant was aged for 30mins, then filtered, washed to neutral and dried at 105 ^oC. The dried product was calcined for 120 min at 450 ^oC in a nitrogen atmosphere. The mass content of nickel was 5% and the mass ratio of ACF and γ-Al_2O_3 was 1:1. The detailed preparation process for the catalyst Ni-Al_2O_3/ACF could be found in our previous work [22].

2.2 Thermodynamic equilibrium analysis

Thermodynamics and kinetics are two key factors controlling the target products of biomass gasification. The effects of gas components, reforming conditions and different reactions on products distribution under

thermodynamic equilibrium were determined by Gibbs free energy minimization method [23, 24]. The total Gibbs free energy of chemical reaction system [25, 26] can be defined as follows:

$$G^t = \sum_{i=1}^{N} n_i \mu_i \tag{1}$$

$$\mu_i = G_{f_i}^o + RTln(\hat{f}_i / f_i^\theta) \tag{2}$$

Where G^t is the total Gibbs free energy of system; n_i is the molar number of different components; μ_i is the chemical potential of different components; G_i^0 is the standard Gibbs free energy; R is the molar gas constant; T is the temperature of reaction system, K; f_i is the fugacity coefficient of different component; f_i^0 is the fugacity coefficient of different component under standard conditions;

The above equation can be transformed by Lagrange multiplier method, and the total Gibbs free energy ΔG^t of the system under equilibrium state satisfies the following requirements [27]:

$$\sum_i^N n_i \left(\Delta G_{f_i}^0 + RTln(\hat{f}_i / f_i^\theta) + \sum_k \lambda_i a_{i,k} \right) = 0 \tag{3}$$

Where λ_i is the Lagrange multiplier; $a_{i,k}$ is the number of atoms of corresponding elements in molecules of different components.

The major gas species involved in the reforming process are H_2, CO, CO_2, H_2O and CH_4 which are served as the simulated biomass derived gas. The conversion ratio of reactants and the yield of products (H_2 or CO) are defined as follows:

$$\chi_{CH_4} = \frac{F_{CH_4,in} - F_{CH_4,out}}{F_{CH_4,in}} \times 100\% \tag{4}$$

$$\chi_{CO_2} = \frac{F_{CO_2,in} - F_{CO_2,out}}{F_{CO_2,in}} \times 100\% \tag{5}$$

$$\chi_{H_2O} = \frac{F_{H_2O,in} - F_{H_2O,out}}{F_{H_2O,in}} \times 100\% \tag{6}$$

$$\chi_{CO} = \frac{F_{CO,out} - F_{CO,in}}{F_{CO,in}} \times 100\% \tag{7}$$

$$\chi_{H_2} = \frac{F_{H_2,out} - F_{H_2,in}}{F_{H_2,in}} \times 100\% \tag{8}$$

Where χ_i represents the conversion rate or yield of different components; $F_{i,in}$ represents flow rate in feed gas, and $F_{j,out}$ is the flow rate in the out products, mL/min.

The Aspen Plus software was applied to conduct the thermodynamic equilibrium analysis. And the flow chart of thermodynamic analysis is shown in Figure S1, which contains unit system selection, model establishment,

component definition, model parameter setting, sensitivity analysis and other processes.

2.2 Macro-kinetics analysis of catalysts

In our previous research [22], it's proved that the ACF in catalyst Ni-Al_2O_3/ACF is favor for the catalytic performance of catalyst in terms of textural properties and surface characteristics. In this study the promotion of activated carbon fibers in catalyst Ni-Al_2O_3/ACF on the catalytic performance of nickel-based alumina will be explained from the perspective of activation energy by macro-kinetics analysis.

A fixed bed reactor [22] was applied for the macro-kinetics analysis of catalysts for the reforming of simulated biomass derived gas. And the cylinder gas was used to simulate the biomass derived gas. 0.5 g of the catalyst Ni-Al_2O_3/ACF with size between 60 and 80 mesh was loaded into a stainless steel pipe whose diameter was 8 mm. Before experiment, the catalysts were reduced in a stream of 50 mL/min of pure H_2 at 650 ^oC for 2 h and then flushed under 50 mL/min of N_2 at the same temperature. The gas flow rates at different temperatures were determined by maintaining a constant flow rate of one reactant and varied other reactants. N_2 was served as a balance gas to maintain atmospheric pressure and kept the total flow constant. The gas composition was determined by the gas chromatography (GC5890, China). The flow rate and temperature were controlled by the mass flow controller and temperature programmed controller respectively. The effects of different parameters such as temperature and components were then determined. Based on the experimental results, a simple power-law type kinetic equation of the catalyst Ni-Al_2O_3/ACF can be calculated. The activation energy within different temperature ranges were also determined based on the Arrhenius equation [28, 29].

3 Results and discussion

3.1 Thermodynamics Analysis

Based on the previous research [8-10], the biomass derived gases are summarized as the supporting information in Table S1. Then the simulated initial components of biomass derived gases is simplified as shown in Table 1. In

this study, the oxygen-to-carbon ratio in all the different feed gas compositions used was either equal to or greater than unity, which indicates that there was enough oxygen to oxidize and prevent formation of solid carbon [30, 31]. Hence, carbon formation was omitted from equilibrium expressions. In addition, methane was considered as the only hydrocarbon. So the major reactions involved in reforming are steam reforming of methane (SRM), dry reforming of methane (DRM) and reverse water-gas shift reaction (RWGS).

Table 1 Simulated initial components of biomass derived gas

Components	H_2	CO	CH_4	CO_2	N_2	H_2O (g)
Volume fraction (%)	12	20	6	12	50	0
Volume flow (mL/min)	120	200	60	120	500	0

3.1.1 Effect of reaction temperature

To reveal the effect of temperature on biomass derived gas reforming, the reformed products were calculated using by Gibbs free energy minimization method between 300 °C and 1600 °C at 0.1 MPa and the results are shown in Figure 1. The ratio of CH_4 to CO_2 is 1:2. In this section steam was not added to the raw input gas. Therefore the reactions in the reforming system are DRM and RWGS.

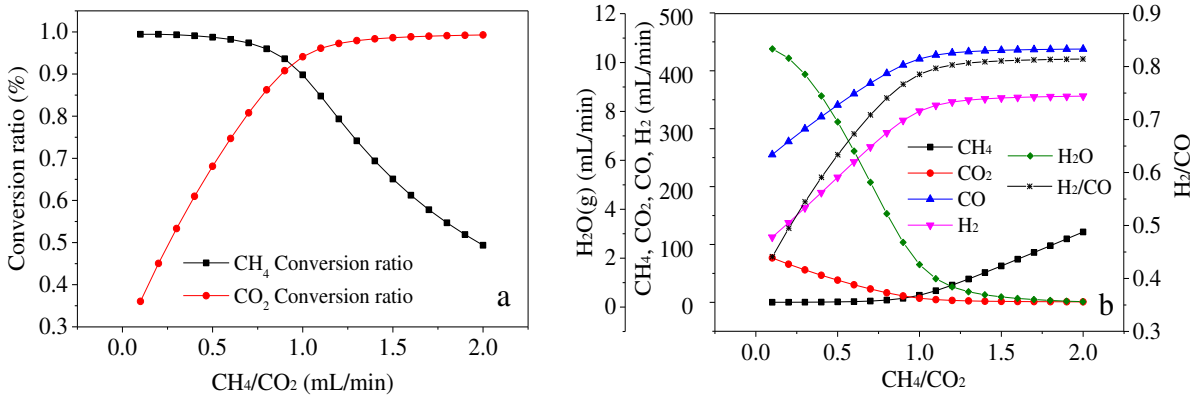

Figure 1 Effects of temperature on flow rate and conversion rate of products (a: Conversion ratio; b: Flow rate of products)

As can be seen from Figure 1 (a), with the increasing of temperature both the conversion ratio of CH_4 and CO_2 changes from negative to positive which indicates that the dry reforming of methane in the system changes from reverse to positive. The changing temperature node is near 600 °C. In addition, when the temperature reaches to

higher than 800 °C, the conversion ratio of CH_4 is near 100%. The RWGS reaction occurs between extra CO_2 and H_2 which leads to the slow increase of CO_2 conversion ratio. Based on Figure 1 (b), with the increasing of temperature the CO yield in products firstly increases remarkably then slightly. While the H_2 decreases slightly at high temperatures. It should be noted that the reaction RWGS plays an important role in the gasified biomass product gas reforming system based on Figure 1 (b). At low temperature, the reactions, WGS and methanation, would occur thus leading to the consumption of CO and the increased ratio of H_2/CO. While at higher temperature over 800 °C, the reaction WGS turns to RWGS which can consume the H_2 thus leading to the decreased ratio of H_2/CO and increase of H_2O. Generally, the H_2 yield is the highest in products around 800 ℃, where the conversion ratio of CH_4 is near 100%. In terms of obtaining H_2-rich gas, 800 ℃ is the optimum reforming temperature for biomass derived primary gas. But in terms of obtaining syngas with low hydrogen-carbon ratio, the reforming temperature should be over 800 ℃, where the ratio of H_2/CO can be adjusted by the reaction RWGS. Based on the analysis of the effect of reaction temperature, improving existing catalysts which can realize the synergistic catalysis for water-gas shift reaction and methane reforming can be a sufficient alternative way applied for the reforming of biomass derived gas.

3.1.2 Effect of ratio of CH_4 to CO_2

The component CO_2 plays an important role in the products distribution during the reforming of biomass derived gas. To illustrate the effect of the ratio of CH_4 to CO_2 on biomass derived gas reforming, the flow rate of CO_2 serves as a fixed value, N_2 serves as the balance gas to maintain the total flow rate constant when CH_4 is changed so as to obtain the different ratio of CH_4 to CO_2 between 0.1 and 2. The products distribution under thermodynamic equilibrium reformed at 800 °C is shown in Figure 2. When the ratio of CH_4 to CO_2 increases, which means that the CH_4 in the reforming system is excess, the conversion ratio of CH_4 decreases, while the conversion rate of CO_2 increases rapidly until completely transformed. As can be seen from Figure 2 (b), the amount of H_2 and CO, as well as the ratio of H_2/CO gradually increase with the increasing of the ratio of CH_4 to CO_2. In addition the amount of

steam in products decreases. At 800℃, the occurred reaction RWGS results in the ratio of H_2/CO less than 1. But the extra CH_4 would consume CO_2 which is unfavorable for the reaction RWGS and increase the ratio of H_2/CO [32]. It's concluded that to increase the amount of syngas and the ratio of H_2/CO, the ratio of CH_4 to CO_2 must be increased appropriately at 800 C.

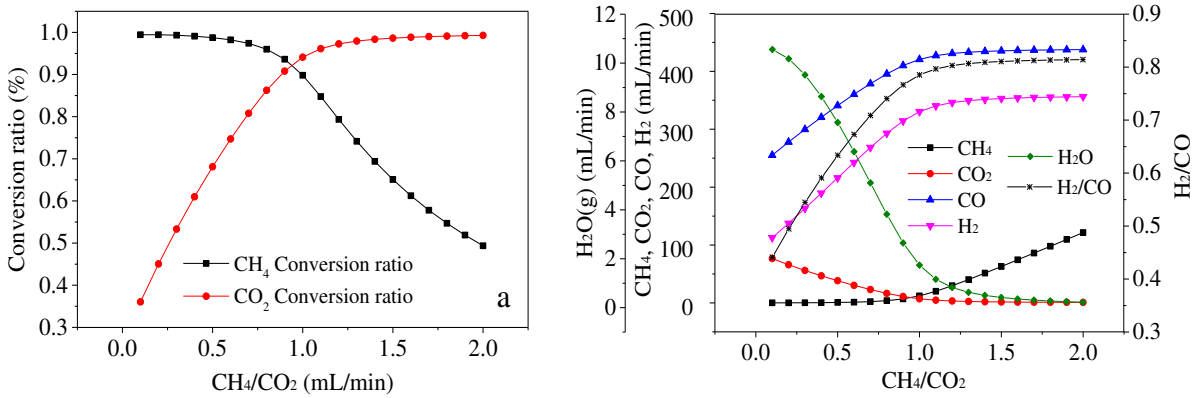

Figure 2 Effects of ratio of CH_4/CO_2 on flow rate and conversion rate of products (a: Conversion ratio; b: Flow rate of products)

3.1.3 Effect of steam

In the process of biomass derived gas reforming, the addition of steam has a significant influence on the products distribution. To reveal the effect of steam on the biomass derived gas reforming process, the influence of various flow rates of steam in the raw input gas was determined. The flow rates of CO_2 and CH_4 served as fixed values and N_2 served as the balance gas to maintain the total gas as constant when the steam input was changed. At 800 ºC, the reactions within the system include DRM, SRM and RWGS. The results of the various gas products produced under thermodynamic equilibrium are shown in Figure 3.

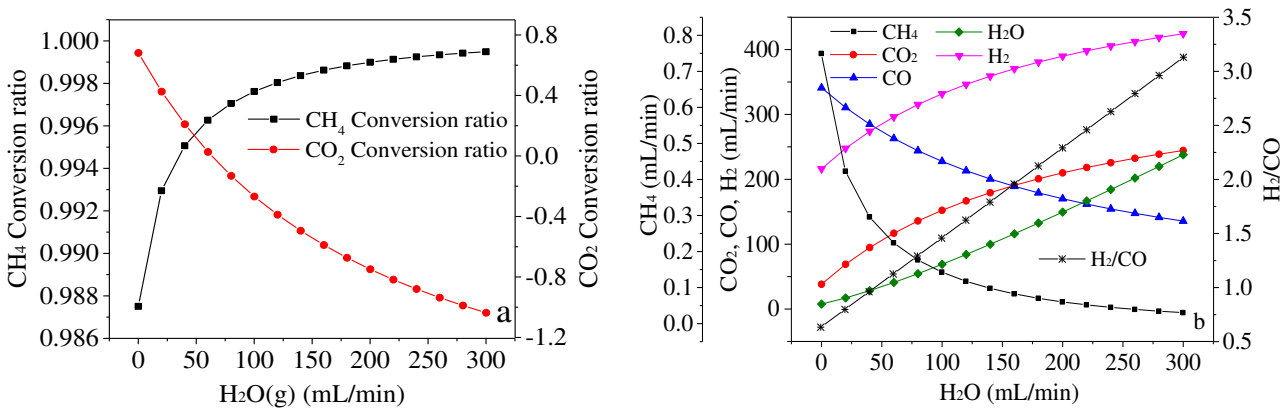

Figure 3 Effects of flow rate of vapor on flow rate and conversion rate of products at 800℃(a: Conversion ratio; b: Flow rate of products)

It's noted in Figure 3 (a) that the CH_4 conversion ratio increases to near 100% while CO_2 conversion ratio decreases with the increased input of steam. The added steam leads to the competing consumption of CH_4 between SRM and DRM which leads to the decreased conversion ratio of CO_2. From Figure 3 (b), it is observed that both the yield of H_2 and CO, and the ratio of H_2/CO increase because of the added steam. The reaction SRM easily occurs because of the lower endothermic value compared with the reaction DRM which leads to the increased ratio of H_2/CO. Therefore, it can be concluded that adding steam into the reforming system of biomass derived gas can adjust the ratio of H_2/CO [33].

To thoroughly illustrate the effect of steam on the reforming process, the temperature range investigated was extended from 600 °C to 1050 °C. At different temperatures the gas products distribution under thermodynamic equilibrium after adding steam into raw gas is shown in Figure 4. When changing the temperature and keeping steam at a different fixed value, it is observed that the conversion ratio of CH_4 increases rapidly near to 100% and the CO keeps increasing while H_2 firstly increases then decreases. This is consistent with the results of Figure 1, but the ratio of H_2/CO shows a different trend. When the added amount of steam in the reforming system is low, with the increasing of temperature the ratio of H_2/CO increases rapidly then slowly declines. The WGS would consume CO and SRM would produce extra H_2 at relatively low temperature thus leading to the increased ratio of H_2/CO. While at higher

temperature over 800 °C, the WGS turns to RWGS which can consume the H_2 thus leading to the decreased ratio of H_2/CO and increase of H_2O. When the amount of steam is excessive, the ratio of H_2/CO appears to decrease directly. The extra steam is favored for the reaction SR and decreases the conversion ratio of CO_2. The reaction RWGS is promoted thus leading directly to the decreased ratio of H_2/CO.

Besides, when changing the added amount of steam and keeping reaction temperature a different fixed value, no matter what the temperature was, the added steam would increase the conversion ratio of CH_4 as well as the amount of H_2 and decrease the conversion ratio of CO_2 as well as the amount of CO. However, the ratio of H_2/CO appears with a different phenomenon under these conditions. At lower temperature, especially below 800 °C, the ratio of H_2/CO increases with the increasing of the amount of steam. While adding the steam into the reforming system at a relatively high temperature, the ratio of H_2/CO decreases with the increased added steam. This interesting phenomenon could be ascribed to the role of WGS and RWGS at different temperatures. Based on the above analysis, it can be concluded that the temperature and steam play a vital role in adjusting the ratio of H_2/CO during the reforming of biomass derived gas. The desired ratio of H_2/CO can be obtained by maintaining the appropriate temperature and steam amount.

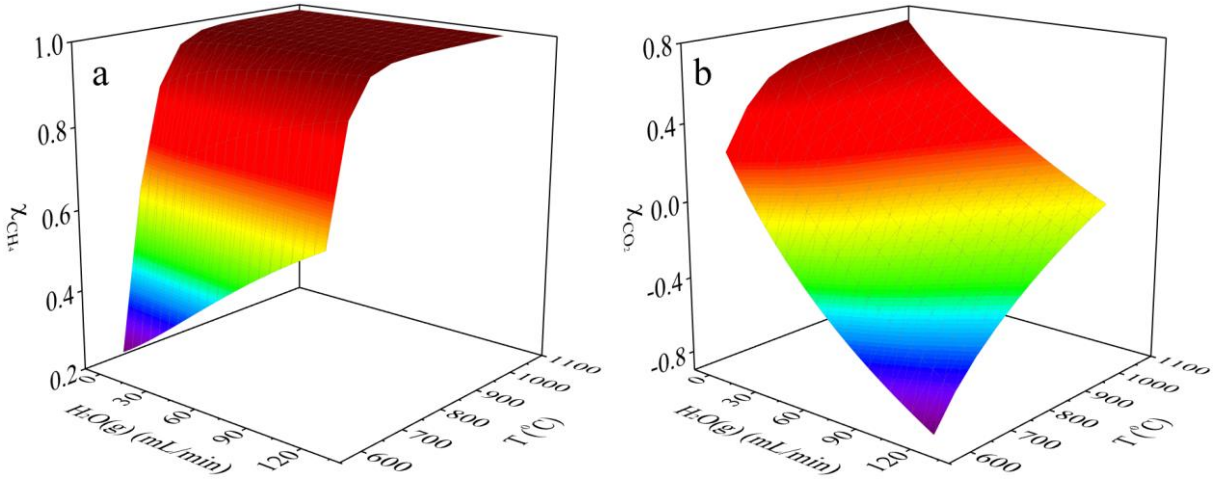

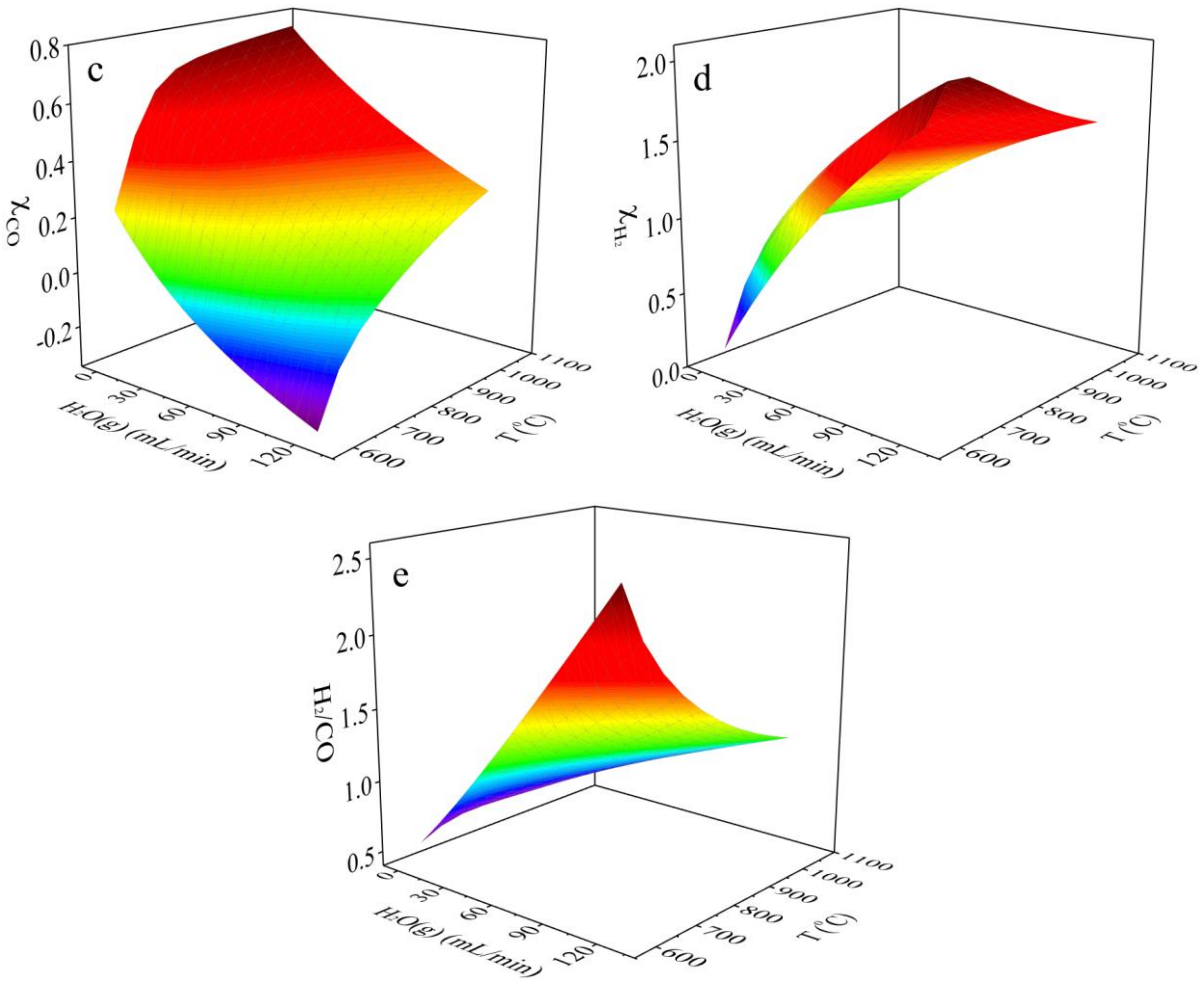

Figure 4 Effects of steam on flow rate and conversion rate of products at different temperature (a: CH_4 Conversion ratio; b: CO_2 Conversion ratio; c: CO increased ratio; d: H_2 increased ratio; e: H_2/CO)

3.2 Macro-kinetics analysis

In our previous research [22], the prepared Ni-Al_2O_3/ACF catalyst was used to reform the simulated biomass derived gas. The catalyst showed excellent catalytic performance because of the addition of ACF based on the analysis of textural properties and surface characteristics. In this section the promotion of activated carbon fibers in catalyst Ni-Al_2O_3/ACF on catalytic performance of nickel-based alumina will be illustrated from the perspective of activation energy by macro-kinetics analysis. A simple power-law type kinetic equation of the catalyst Ni-Al_2O_3/ACF in the reforming system of the simulated biomass derived gas was determined and the apparent activation energy of CH_4 and CO_2 between different temperature ranges was calculated.

3.2.1 Effects of components and calculation of reaction orders

To obtain the reaction orders of different components, the effects of CH_4, CO_2, H_2 and CO with different concentration on the conversion ratio of CH_4 and CO_2 were investigated and the results are shown in Figure 5. The detailed distribution of components in the raw input gas is described in Table S2. It's observed that increasing the amount of raw input gas can promote a positive reaction, conversely, increasing the amount of produced gas will inhibit the reaction going forward. However, it's noted that in Figure 5 the conversion ratio of CO_2 and CH_4 is greatly influenced by the concentration of CO_2 and CH_4 while less affected by H_2 and CO.

In addition, the effects of CH_4, CO_2 with different concentration on the ratio of H_2/CO were also shown in Figure S2. With the increasing of CH_4 in raw gas, the ratio of H_2/CO in gas products also increases gradually. In this process, compared with the amount of CO_2, the CH_4 concentration ranges from insufficient to excessive. When the amount of CH_4 is less than CO_2, the excess CO_2 will react with H_2 and ACF during reforming, which leads to the consumption of H_2 and generation of CO. At this time, the ratio of H_2/CO is relatively low. When the CH_4 concentration increases gradually, or even excessively, these two reactions can be inhibited, and excessive CH_4 will crack and generate H_2, which leads to the increased ratio of H_2/CO.

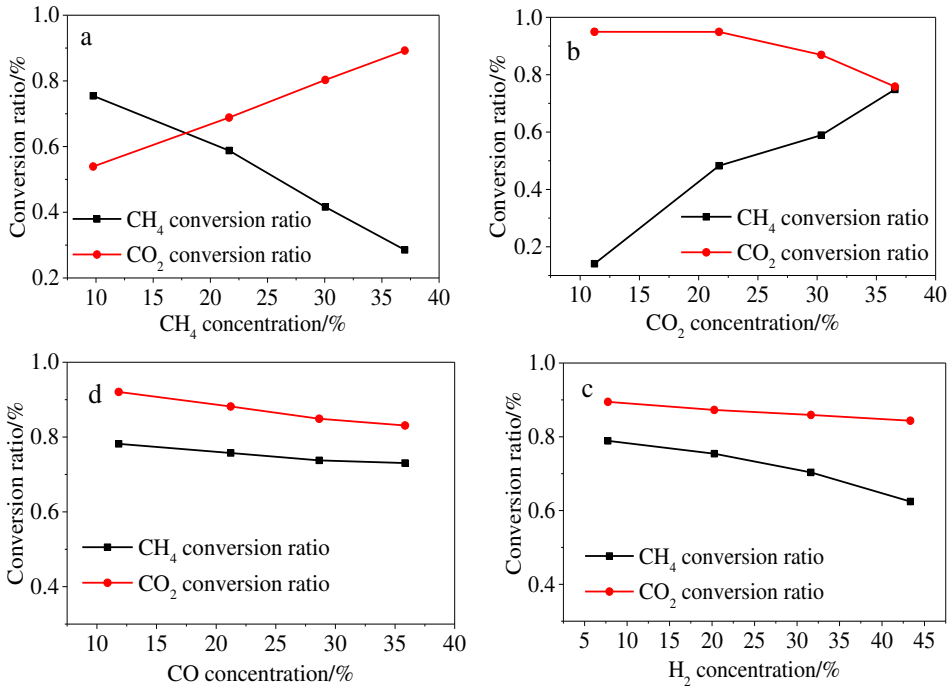

Figure 5 Effects of different components on the conversion ratio of CH_4 and CO_2（Catalyst dosage: 0.5 g; Reaction temperature: 800 °C; WHSV: 24000 mL•h^{-1}•gcat^{-1}）

The simple power-law type kinetic equation is described as follows,

$$r_{CH_4} = k x_{in,CH_4}^{n_1} x_{in,CO_2}^{n_2} x_{in,CO}^{n_3} x_{in,H_2}^{n_4} \tag{6}$$

$$r_{CH_4} = WHSV * (x_{in,CH_4} - x_{out,CH_4}), \quad x_{i,j} = \frac{F_{i,i}}{F_i} \tag{7}$$

Where r_{CH_4} is the reaction rate, mL•h^{-1}•gcat^{-1}; n_j is the reaction order of different components; k is the reaction rate constant; $WHSV$ is the Weight Hour Space Velocity, mL•h^{-1}•gcat^{-1}; $x_{i,j}$ is the concentration of different inlet or outlet components; $F_{i,i}$ is the flow rate of different inlet or outlet components, mL•h^{-1}; F_i is the total flow rate of inlet or outlet, mL•h^{-1}.

Taking the logarithm for the kinetic equation (6) to convert simple power-law type to a linear equation as follows,

$$\ln r_{CH_4} = \ln k + n_1 \ln x_{in,CH_4} + n_2 \ln x_{in,CO_2} + n_3 \ln x_{in,CO} + n_4 \ln x_{in,H_2} \tag{8}$$

Based on the results of Figure 5, the related parameters in equation (8) were calculated. Taking the calculation of the reaction order of CH_4 as an example, changing the concentration of CH_4 with a fixed concentration of other components, equation (8) is simplified as follows,

$$\ln r_{CH_4} = n_1 \ln x_{in,CH_4} + C \tag{9}$$

Where C is the constant term. The reaction order may be obtained by graphical method as shown in Figure S3 (a). The slope of the straight line of equation (9) is the reaction order of CH_4, and some of the other three reaction orders of CO_2, CO and H_2 are obtained by the same way. The results are shown in Figure S3. The reaction orders are gathered in Table 2. The reaction orders of CH_4, CO_2, CO and H_2 are 0.73005, 0.68782, -0.19126 and -0.04415 respectively. Then the simple power-law type kinetic equation is described as follows.

$$r_{CH_4} = k x_{in,CH_4}^{0.73005} x_{in,CO_2}^{0.68782} x_{in,CO}^{-0.19126} x_{in,H_2}^{-0.04415} \tag{10}$$

Table 2 Reaction orders of different components

Component	CH_4	CO_2	CO	H_2
Reaction order	0.73005	0.68782	-0.19126	-0.04415

3.2.3 Effect of temperature and calculation of apparent activation energy

To obtain the apparent activation energy of CH_4 and CO_2, the effect of temperature on the conversion ratio of CH_4 and CO_2, and the ratio of H_2/CO was investigated and the results are shown in Figure 6. With the increasing of temperature less than 800 ºC, the conversion ratio of CH_4 and CO_2 increases remarkably. When the temperature is over 800 ºC, the conversion ratio increases slowly. This phenomenon, which corresponds with the thermodynamics analysis, suggests that the temperature of around 800 ºC is the point where the reaction WGS turns to RWGS.

Besides, the ratio of H_2/CO also has the same trend. With the increasing of temperature the ratio of H_2/CO increases gradually. At low temperature especially when the temperature is below 800℃, the ratio of H_2/CO is below 1. Because the catalyst is the activated carbon fibers (ACF) supported nickel based alumina. At low temperature, part of ACF will react with CO_2, which could increase the output of CO and decrease the ratio of H_2/CO.

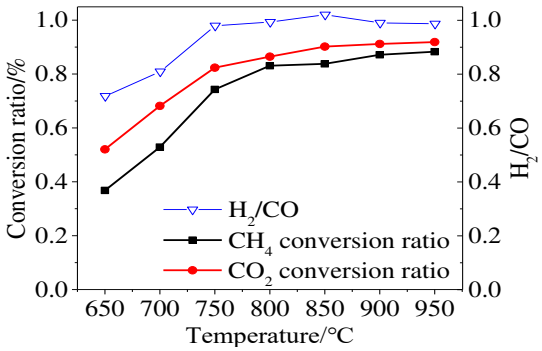

Figure 6 Effect of temperature on the conversion ratio of CH_4 and CO_2（Catalyst dosage: 0.5 g; WHSV: 24000 mL $\bullet h^{-1} \bullet gcat^{-1}$）

Among the reported literatures, the calculation of apparent activation energy are always over a wide temperature range which is not accurate and not consistent with the experimental phenomenon. Based on Figure 6, the effect of temperature on the conversion ratio of CH_4 and CO_2 could be divided into two parts. Therefore, the apparent activation energy may be calculated over two temperature ranges, the first between 650 ºC ~750 ºC and the second

between 800 °C ~950 °C. The calculation of apparent activation energy is based on the logarithmic Arrhenius empirical formula [34, 35] described as follows.

$$\ln k = \ln A - \frac{E_a}{RT} \tag{11}$$

Where A is the pre-exponential factor, $mL \cdot h^{-1} \cdot gcat^{-1}$; E_a is the apparent activation energy, $kJ \cdot moL^{-1}$; R is the molar gas constant, 8.314 $J \cdot moL^{-1} \cdot K^{-1}$.

Taking CH_4 for example, the reaction rate constant k is calculated by the followed equation.

$$k = \frac{r_{CH_4}}{x_{in,CH_4}^{n_1} x_{in,CO_2}^{n_2} x_{in,CO}^{n_3} x_{in,H_2}^{n_4}} = \frac{x_{in,CO}^{0.19126} x_{in,H_2}^{0.04415}}{x_{in,CH_4}^{0.73005} x_{in,CO_2}^{0.68782}} \tag{12}$$

Based on equation (11), the parameters A and E_a of CH_4 and CO_2 were obtained by graphical method as shown in Figure S4. The abscissa axis is 1/T and the ordinate axis is ln$k$. By linearization fitting, the pre-exponential factor and activation energy can be obtained from the slope and intercept of the line. The detailed pre-exponential factor and activation energy results are summarized in Table 3. The detailed simple power-law type kinetic equation is described as follows.

$$r_i = k_i x_{in,CH_4}^{0.73005} x_{in,CO_2}^{0.68782} x_{in,CO}^{-0.19126} x_{in,H_2}^{-0.04415},\ i = \mathbf{CH_4}, \mathbf{CO_2} \tag{13}$$

$$k_{CH_4} = 7.31187 * 10^6 e^{-96.27903/RT},\ k_{CO_2} = 3.38086 * 10^4 e^{-50.44877/RT} \quad T < 800℃ \tag{14}$$

$$k_{CH_4} = 175.30543 e^{-5.3252/RT},\quad k_{CO_2} = 165.05685 e^{-4.69342/RT} \quad T \geq 800℃ \tag{15}$$

Table 3 Pre-exponential factor and apparent activation energy of CH_4 and CO_2

Temperature	CH_4		CO_2	
	A($mL \cdot h^{-1} \cdot gcat^{-1}$)	E_a($kJ \cdot moL^{-1}$)	A ($mL \cdot h^{-1} \cdot gcat^{-1}$)	E_a($kJ \cdot moL^{-1}$)
< 800 °C	7.31187*10^6	96.27903	3.38086*10^4	50.44877
≥ 800 °C	175.30543	5.32520	165.05685	4.69342

Compared with reported results shown in Table 4, the apparent activation energy of CO_2 and CH_4 for the catalyst Ni-Al_2O_3/ACF is lower than the reported nickel based catalysts especially at temperature over 800 °C. In the process of dry reforming of methane, the coke always leads to deactivation of catalyst. It could be ascribed the fact that the dissociation of CO_2 for intermediate oxygen production is slower than the methane decomposition for intermediate

carbon production. Excess intermediate active carbon species will be converted into inert carbon [36, 37]. In terms of activation energy, to reduce carbon deposition, it is necessary to decrease the activation energy of CO_2, which makes it easier to activate CO_2 and dissociate more intermediate oxygen atoms. Figure S5 is the schematic of DRM reaction activation, the addition of ACF in the catalyst Ni-Al_2O_3/ACF decreases the activation energy of CO_2 remarkably which suggests that the catalyst can effectively accelerate the carbon removal reaction and thus inhibits the carbon deposition during the dry reforming of methane.

Table 4 Comparison of apparent activation energy

Catalysts	Ea(kJ/moL)		Reference
	CH_4	CO_2	
Ni/SiO_2	96.27	79.53	[34]
Ni/MgO	92.09	87.90	[34]
Ni/TiO_2	108.83	87.90	[34]
Ni/Al_2O_3	70.74	69.07	[35]
Ni/CaO-Al_2O_3	106.74	98.79	[33]
Pt-Ni/Al_2O_3	111.34	70.74	[38]
Ni-Al_2O_3/ACF (< 800 °C)	96.28	50.45	This work
Ni-Al_2O_3/ACF (≥ 800 °C)	5.33	4.69	

4 Conclusion

In this study, the thermodynamic analysis was carried out for simulated biomass derived gas to optimize the reforming conditions so as to obtain more syngas with appropriate ratio of H_2 to CO. And the macroscopic reaction kinetics of catalyst Ni-γ-Al_2O_3/ACF was investigated to illustrate the influence of ACF on catalytic reforming performance of simulated biomass derived gas in terms of activation energy. Some conclusions can be derived as follows. The temperature and steam play an important role in adjusting the ratio of H_2/CO in syngas from biomass derived gas reforming. 800 ℃ is the optimum reforming temperature for biomass derived primary gas to obtain H_2-rich gas. But in terms of obtaining syngas with low hydrogen-carbon ratio, the reforming temperature should be over 800 ℃, where the ratio of H_2/CO can be adjusted by the reaction RWGS. By changing the temperature and the steam amount, the reaction RWGS can occur in different directions so as to adjust the ratio which can meet different desired

application requirements. In addition, for the catalyst Ni-γ-Al_2O_3/ACF, the apparent activation energy of CH_4 and CO_2 are 96.28 kJ•moL^{-1} and 50.45 kJ•moL^{-1} below 800 °C, 5.33 kJ•moL^{-1} and 4.69 kJ•moL^{-1} over 800 °C respectively. The apparent activation energy of CO_2 is lower than other catalysts reported in the literatures especially at temperature over 800 °C which suggests that the catalyst favors the activation of CO_2 and can effectively inhibit carbon deposition.

Supplementary material

A Word document containing Table S1, Table S2, Figure S1, Figure S2, Figure S3, Figure S4 and Figure S5.

Acknowledgements

This work was supported by the National Natural Science Foundation of China [grant number 51576048]; and the Fundamental Research Funds for the Central Universities; the Postgraduate Research & Practice Innovation Program of Jiangsu Province [grant number KYCX17_0082].

References

[1] Wei Y, Song M, Yu L, Gao R, Meng F, Xiao J, Zhang Y (2018) Promotion effect of SiO_2 on the catalytic performance of Ni/CF for biomass derived gas reforming. Ind Eng Chem Res 57(32): 10851-10858.

[2] Kathiraser Y, Wang Z, Kawi S (2013) Oxidative CO_2 Reforming of Methane in $La_{0.6}Sr_{0.4}Co_{0.8}Ga_{0.2}O_{3-\delta}$ (LSCG) Hollow Fiber Membrane Reactor. Environ Sci Technol 47(24): 14510-14517.

[3] Ma Z, Bai J, Bai Z, Kong L, Guo Z, Yan J, Li W (2014) Mineral Transformation in Char and Its Effect on Coal Char Gasification Reactivity at High Temperatures, Part 2: Char Gasification. Energ Fuel 28(3): 1846-1853.

[4] Bai J, Li W, Bai Z (2011) Effects of Mineral Matter and Coal Blending on Gasification. Energ Fuel 25(3): 1127-1131.

[5] Chen C, Zhang S, Xu K, Luo G, Yao H (2016) Experimental and Modeling Study of Char Gasification with Mixtures of CO_2 and H_2O. Energ Fuel 30(3): 1628-1635.

[6] Cao JP, Liu TL, Ren J, Zhao XY, Wu Y, Wang JX, Ren XY, Wei XY (2017) Preparation and characterization of

nickel loaded on resin char as tar reforming catalyst for biomass gasification. J Anal Appl Pyrol 127: 82-90.

[7] Tilay A, Azargohar R, Gerspacher R, Dalai A, Kozinski J (2014) Gasification of canola meal and factors affecting gasification process. Bioenerg Res 7(4): 1131-1143.

[8] Dong L, Wu C, Ling H, Shi J, Williams PT, Huang J (2016) Development of Fe-promoted Ni-Al catalysts for hydrogen production from gasification of wood sawdust. Energ Fuel 31(3): 2118-2127.

[9] Waheed QM, Wu C, Williams PT (2016) Pyrolysis/reforming of rice husks with a Ni-dolomite catalyst: Influence of process conditions on syngas and hydrogen yield. J Energy Inst 89(4): 657-667.

[10] Wu C, Williams PT (2009) Hydrogen production by steam gasification of polypropylene with various nickel catalysts. Appl Catal B-Environ 87(3-4): 152-161.

[11] Wu C, Budarin VL, Wang M, Sharifi V, Gronnow MJ, Wu Y, Swithenbank J, Clark JH, Williams PT (2015) CO_2 gasification of bio-char derived from conventional and microwave pyrolysis. Appl Energ 157: 533-539.

[12] Waheed QM, Wu C, Williams PT (2016) Hydrogen production from high temperature steam catalytic gasification of bio-char. J Energy Inst 89(2): 222-230.

[13] Aydin ES, Yucel O, Sadikoglu H (2018) Numerical and experimental investigation of hydrogen-rich syngas production via biomass gasification. Int J Hydrogen Energ 43(2): 1105-1115.

[14] Chan FL, Tanksale A (2014) Review of recent developments in Ni-based catalysts for biomass gasification. Renew Sust Energ Rev 38: 428-438.

[15] Wen J, Lin H, Han X, Zheng Y, Chu W (2017) Physicochemical Studies of Adsorptive Denitrogenation by Oxidized Activated Carbons. Ind Eng Chem Res 56(17): 5033-5041.

[16] Wang BS, Cao JP, Zhao XY, Bian Y, Song C, Zhao YP, Fan X, Wei XY, Takarada T (2015) Preparation of nickel-loaded on lignite char for catalytic gasification of biomass. Fuel Process Technol 136: 17-24.

[17] Yao D, Hu Q, Wang D, Yang H, Wu C, Wang X, Chen H (2016) Hydrogen production from biomass gasification

using biochar as a catalyst/support. Bioresource Technol 216: 159-164.

[18] Song M, Jin B, Xiao R, Yang L, Wu Y, Zhong Z, Huang Y (2013) The comparison of two activation techniques to prepare activated carbon from corn cob. Biomass Bioenerg 48: 250-256.

[19] Meng F, Song M, Wei Y, Wang Y (2019) The contribution of oxygen-containing functional groups to the gas-phase adsorption of volatile organic compounds with different polarities onto lignin-derived activated carbon fibers. Environ Sci Pollut Res 26(7): 7195-7204.

[20] Wei Y, Song M, Yu L, Tang X (2017) Preparation of ZnO-Loaded Lignin-Based Carbon Fiber for the Electrocatalytic Oxidation of Hydroquinone. Catalysts 7(6): 180.

[21] Song M, Zhang W, Chen Y, Luo J, John CC (2017) The preparation and performance of lignin-based activated carbon fiber adsorbents for treating gaseous streams. Front Chem Sci Eng 11(3): 328-337.

[22] Yu L, Song M, Wei Y, Xiao J (2018) Combining carbon fibers with Ni/γ-Al_2O_3 used for syngas production: Part A: preparation and evaluation of complex carrier catalysts. Catalysts 8: 658.

[23] Leal AM, Kulik DA, Kosakowski G (2016) Computational methods for reactive transport modeling: A Gibbs energy minimization approach for multiphase equilibrium calculations. Adv Water Resour 88: 231-240.

[24] Jafarbegloo M, Tarlani A, Mesbah AW, Sahebdelfar S (2015) Thermodynamic analysis of carbon dioxide reforming of methane and its practical relevance. Int J Hydrogen Energ 40(6): 2445-2451.

[25] Tabrizi FF, Mousavi SAHS, Atashi H. (2015) Thermodynamic analysis of steam reforming of methane with statistical approaches. Energ Convers Manage 103: 1065-1077.

[26] Jang WJ, Jeong DW, Shim JO, Kim HM, Roh HS, Son IH, Lee SJ. (2016) Combined steam and carbon dioxide reforming of methane and side reactions: Thermodynamic equilibrium analysis and experimental application. Appl Energ 173:80-91.

[27] Li Y, Wang Y, Zhang X, Mi Z. (2008) Thermodynamic analysis of autothermal steam and CO_2 reforming of

methane. Int J Hydrogen Energ 33(10): 2507-2514.

[28] Polo-Garzon F, Scott JK, Bruce DA (2016) Microkinetic model for the dry reforming of methane on Rh doped pyrochlore catalysts. J Catal 340: 196-204.

[29] Nguyen TH, Łamacz A, Krztoń A, Ura A, Chałupka K, Nowosielska M, Rynkowski J, Djéga-Mariadassou G (2015) Partial oxidation of methane over NiO/La_2O_3 bifunctional catalyst II: Global kinetics of methane total oxidation, dry reforming and partial oxidation. Appl Catal B-Environ 165: 389-398.

[30] Yang M, Papp H (2006) CO_2 reforming of methane to syngas over highly active and stable Pt/MgO catalysts. Catal Today 115(1): 199-204.

[31] Özkara-Aydınoğlu Ş, Özensoy E, Aksoylu AE (2009) The effect of impregnation strategy on methane dry reforming activity of Ce promoted Pt/ZrO. Int J Hydrogen Energ 34(24): 9711-9722.

[32] Nandini A, Pant KK, Dhingra SC (2006) Kinetic study of the catalytic carbon dioxide reforming of methane to synthesis gas over Ni-K/CeO_2- Al_2O_3 catalyst. Appl Catal A-Gen 308: 119-127.

[33] Lemonidou AA, Vasalos IA (2002) Carbon dioxide reforming of methane over 5wt.% Ni/CaO-Al_2O_3 catalyst. Appl Catal A-Gen 228(1): 227-235.

[34] Wei J, Iglesia E (2004) Isotopic and kinetic assessment of the mechanism of reactions of CH_4 with CO_2 or H_2O to form synthesis gas and carbon on nickel catalysts. J Catal 224(2): 370-383.

[35] Aparicio LM (1997) Transient Isotopic Studies and Microkinetic Modeling of Methane Reforming over Nickel Catalysts. J Catal 165(2): 262-274.

[36] Liu D, Wang Y, Shi D, Jia X, Wang X, Borgna A, Lau R, Yang Y (2012). Methane reforming with carbon dioxide over a Ni/ZiO_2-SiO_2 catalyst: Influence of pretreatment gas atmospheres. Int J Hydrogen Energ 37(13): 10135-10144.

[37] Liu D, Quek XY, Cheo WNE, Lau R, Borgna A, Yang Y (2009). MCM-41 supported nickel-based bimetallic

catalysts with superior stability during carbon dioxide reforming of methane: effect of strong metal-support interaction. J Catal 266(2): 380-390.

[38] Özkara-Aydınoğlu Ş, Aksoylu AE (2013) A comparative study on the kinetics of carbon dioxide reforming of methane over Pt-Ni/Al_2O_3 catalyst: Effect of Pt/Ni Ratio. Chem Eng J 215: 542-549